




Hydro-mechanical coupled analysis of near-wellbore fines migration from unconsolidated reservoirs

Fengshou Zhang^{1,2} · Tuo Wang^{1,2} · Fang Liu^{1,2,3}  · Ming Peng^{1,2} · Bate Bate^{4,5} · Pei Wang⁶

Received: 14 September 2020 / Accepted: 10 October 2021 / Published online: 4 January 2022
© The Author(s), under exclusive licence to Springer-Verlag GmbH Germany, part of Springer Nature 2022

Abstract

Oil or gas production from unconsolidated reservoirs could be hampered by sand migration near the wellbore. This paper presents a numerical investigation of production-induced migration of fine sands towards a wellbore drilled in a gap-graded sediment. The solid–fluid interaction is simulated by coupling the discrete element method and the dynamic fluid mesh. With the merit of DEM and a dynamic mesh, the model is capable of naturally capturing particle movements and spatiotemporal variations of hydraulic properties of the sediment at the pore scale. The results show that fine particles are mobilized by radial flow under an imposed hydraulic gradient, and the increase in the hydraulic gradient causes an increase in the fines production. The microscopic pattern of sand migration is clearly visualized through the simulation. The presence of fine particles affects the process of fines migration through two competing mechanisms. Under a low fine content, fine sands mainly serve as the fines production source, and thus, fines production is enhanced as the fine content increases up to a critical value, beyond which fines production is weakened with a further increase in the fine content since the blocking effect gradually dominates. A barrier layer is likely formed during sand migration due to settling and jamming of fine sands at the throats of pores, as fine sands migrate with the radial flow towards the wellbore. This layer is helpful to slow down sand migration, while it could impede production due to reduced permeability in the affected reservoir.

Keywords DEM · Dynamic fluid mesh · Fines migration · Unconsolidated reservoir

✉ Fang Liu
liufang@tongji.edu.cn

- ¹ Key Laboratory of Geotechnical & Underground Engineering of Ministry of Education, Tongji University, Shanghai 200092, China
- ² Department of Geotechnical Engineering, College of Civil Engineering, Tongji University, Shanghai 200092, China
- ³ State Key Laboratory of Disaster Reduction in Civil Engineering, Tongji University, Shanghai 200092, China
- ⁴ Institute of Geotechnical Engineering, College of Civil Engineering and Architecture, Zhejiang University, Hangzhou 310058, China
- ⁵ MOE Key Laboratory of Soft Soils and Geoenvironmental Engineering, Zhejiang University, Hangzhou 310058, China
- ⁶ Department of Civil and Environmental Engineering, The Hong Kong Polytechnic University, Hung Hom, Kowloon, Hong Kong 999077, China

1 Introduction

Reservoirs that consist of high-permeability soft formation such as non-crystalline rock and sands are widely distributed in the world [17, 21]. These unconsolidated reservoirs are susceptible to fines migration due to drag forces during production [47]. Mobilized under high-pressure gradients, fine particles that are present originally or derived from disaggregation of the unconsolidated matrix migrate through and sometimes dislodge in the porous load-bearing matrix, causing variations in the pore structure and thus the fluid conductivity of the reservoirs [26, 29]. The moving fine particles can erode downhole and surface equipment, and even pose potential risks of limited productivity and well failure due to invasion of fine particles through wellbores, i.e. the so-called phenomenon of fines production. Excessive fines production caused detrimental effects on conventional well production [15, 30, 41], and also forced premature termination of production from methane hydrates reservoirs [11, 24].

Therefore, there is always a cost benefit if fines migration modelling is implemented early to improve the fundamental understanding of near-wellbore behaviour of migrating fine particles.

Extensive experimental studies have been conducted to model fines migration in controllable conditions [6, 7, 12, 32, 37]. To achieve convergent radial flow, which is the prevailing flow condition in gas or oil production, Valdes and Santamarina [39] developed a disc-shaped device to simulate particle migration caused by near-wellbore radial flow. Limited by experimental setup, the test was carried out under low stress conditions, while the in situ formation pressure is much higher. Han et al. [20] enabled a model test of fines production in high-pressure formation with a high-pressure vessel driven by axial flow rather than radial flow. Experimental studies facilitated formulation of the criteria of fines migration and the predictive models of fines volume, but they fell short of revealing the migration and retention of fine particles in pores, which is critically important for fundamental understanding of fines migration. Although efforts were made to directly observe particle migration by using fixed cylinders [6, 23] or microfluidic chips [28] to mimic pore throats in two dimensions, tracing movement of fine particles in a 3D flow through a realistic formation remains extremely challenging.

Besides experimental studies, numerical simulation is a useful tool to study fines migration [1, 16, 34], and especially powerful to visualize fluid flow and solid migration. Compared to the continuum-based models that are thoroughly reviewed by Rahmati et al. [31], the discrete element method (DEM) can naturally capture grain-scale movements of constituent particles of a sediment, and therefore, it is ideal for modelling fines migration once it is equipped with fluid flow analysis. The common DEM–fluid coupling methods include lattice Boltzmann method (LBM) and computational fluid dynamics (CFD) [4, 5, 14, 43, 46]. Han and Cundall [19] developed a DEM–LBM model to investigate fines migration from perforation cavities. The major drawback of the DEM–LBM coupling system is that it is computationally expensive to simulate models with lots of particles. Li et al. revealed the mechanism of sand production on the grain scale by combining DEM and CFD [27]. Grof et al. [18] and Climent et al. [10] developed a DEM–CFD model to investigate particle migration. The traditional DEM–CFD coupled model is based on a coarse grid to simulate the interaction between fluid and solid particles, which cannot resolve the fluid flow at the pore scale and therefore is inaccurate to simulate fine sand migration among coarse particles in unconsolidated reservoirs consisting of gap-graded soils. Zhang et al. [45] developed a new fluid–solid coupled numerical scheme by combining the dynamic fluid mesh (DFM) method with

DEM. This scheme dynamically constructs a fluid mesh based on moving centres of coarse particles. It proves effective for capturing the variation of porosity due to soil skeleton deformation and particle loss, and enables pore-scale analyses of fluid flow and solid migration [45].

Considering the merit of combining DFM and DEM, we employ this scheme to investigate the mechanism of fines migration near a wellbore drilling into a deformable porous medium, i.e. an unconsolidated reservoir composed of gap-graded sediments. A parametric study is performed to identify controlling factors that impact the fines production volume and the spatiotemporal pattern of fines migration. The term “fines” used here is not referred to clay particles but particles relatively small in size. The presented methodology is applicable to clay particles only if the computational cost is affordable for clay particles. However, this application is beyond the scope of this study. This paper is organized as follows. Section 2 briefly introduces the numerical scheme used in this study. Section 3 presents the model setup with model parameters. Section 4 analyses the microscopic processes that control fines migration. Section 5 discusses the effect of several key parameters, followed by conclusions in Sect. 6.

2 The DEM–DFM coupled scheme

The fluid–particle coupled scheme developed by combining DEM and DFM is detailed in our previous study [45], and here we only recap the salient features of the scheme for completeness.

2.1 The workflow

Figure 1 illustrates the workflow of a DEM–DFM coupled simulation for fines migration and production in a gap-graded sediment composed of coarse and fine particles. A DEM model of the sediment (the solid part) enclosed by walls is constructed by using the commercial code PFC3D [22]. A Python script is developed for flow analysis (the fluid part) with DFM and to handle the conversations with the DEM model, including flow meshing according to the DEM model, calculating the fluid–solid interactive forces and passing the forces back to the DEM model. The solid–fluid interactive forces are applied in each step, while the fluid mesh is updated at a pre-determined time interval for efficiency. Here, we assume incompressible fluid following Darcy’s law.

2.2 Meshing and flow analysis

For the flow analysis, the method of Delaunay triangulation is used to discretize the computation domain into a set of

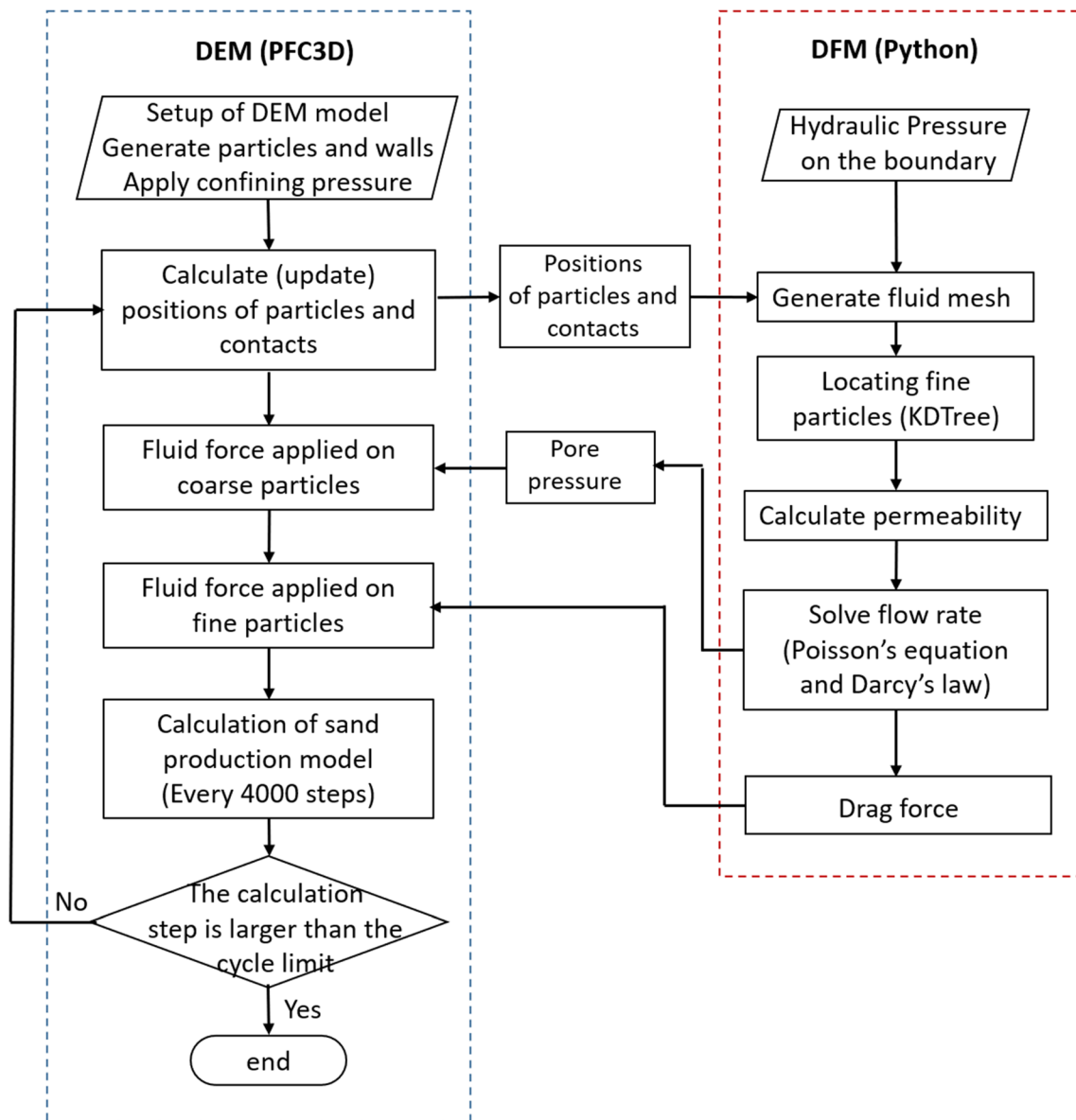


Fig. 1 The workflow of a DEM-DFM coupled simulation for fines production with a gap-graded soil

tetrahedrons [3]. The centroids of the coarse particles and their contact points with boundary walls are used as the vertexes of the tetrahedrons to be constructed. The mesh is updated at a pre-determined time interval as particles move over time.

Once the fluid mesh is generated, we allocate every fine particle to a nearest tetrahedron by using the KDTree algorithm [36]. With the allocated fine particle, a tetrahedron can be divided into four sub-tetrahedrons, each of which is constituted by the fine particle and any three nodes of the parent tetrahedron. The fine particle is considered being enclosed by the tetrahedron, if the total volume of the four sub-tetrahedrons equals the volume of the parent

tetrahedron; otherwise, the procedure is reiterated until a true pair of fine particles and tetrahedrons is found.

The formation properties of unconsolidated reservoirs (e.g. the porosity and the permeability) are determined for each tetrahedron separately to consider heterogeneity in the sediment. The porosity of a tetrahedron is computed as:

$$\phi = \frac{V_{\text{tet}} - V_{\text{coarse}} - V_{\text{fine}}}{V_{\text{tet}}} \quad (1)$$

where V_{tet} is the volume of the tetrahedron, V_{coarse} and V_{fine} represent the volume occupied by the coarse and fine particles within this tetrahedron, respectively. Note that V_{fine} is simply the entire volume of the fine particles enclosed in the tetrahedron, while V_{coarse} is only the

volume inside the tetrahedron rather than the volume of entire coarse particles.

Given the porosity of a tetrahedron, the permeability in the tetrahedron is obtained based on the Kozeny–Carman equation [2]:

$$k = \frac{d_m^2}{180} \frac{\phi^3}{(1 - \phi)^2} \tag{2}$$

where d_m is the average diameter of fine particles in the tetrahedron, and ϕ is the matrix porosity. Note that Eq. (2) is only used to calculate the pore-scale permeability in individual tetrahedrons, the voids formed by coarse particles and filled only with fine particles. Within each of these voids, the permeability is solely controlled by the size of fine particles in addition to the local porosity in each void given in Eq. (1).

According to Darcy’s law, the velocity of the fluid flow in a porous medium is computed as:

$$\mathbf{v} = -\frac{k}{\mu\phi} \nabla p \tag{3}$$

where \mathbf{v} is the fluid velocity, p is the fluid pressure, and μ is the fluid dynamic viscosity.

Assume the fluid is incompressible, thus:

$$\nabla \cdot \mathbf{v} = 0 \tag{4}$$

Combining Eqs. (3) and (4), we reach a Poisson’s equation as:

$$\nabla \cdot \left(\frac{k}{\mu\phi} \nabla p \right) = 0 \tag{5}$$

This equation is solved for piece-wise constant pressure over the fluid elements, using the *fipy* solver, an object-oriented partial differential equation (PDE) solver written in Python based on a standard finite volume (FV) approach [36]. With given boundary conditions, the pressure in each tetrahedron element can be solved. Fluid velocity on every face of the element is derived from Darcy’s law. The fluid velocity at the centre of every element is then computed from interpolation:

$$v_i = \frac{\sum_{j=1}^4 n_{ji} v_{ji} S_j}{\sum_{j=1}^4 n_{ji} S_j}, i = 1, 2, 3 \tag{6}$$

where v_i is the averaged fluid velocity in the i^{th} direction based on the weighted mean from four faces of the tetrahedron, S_j is the area of the j^{th} face of the element, and n_{ji} is the component in the i -direction of the normal vector of the j^{th} face.

2.3 Fluid–particle interactive forces

The flow-induced forces on the coarse and fine particles are considered distinctively. A coarse particle receives pressures from a number of fluid elements it connects, and thus, the resultant force is computed as:

$$\mathbf{f}_c = \sum_i \mathbf{P}_i S_i \tag{7}$$

where \mathbf{P}_i is the pressure in the i^{th} element, and S_i is surface area of the i^{th} element projected on the particle.

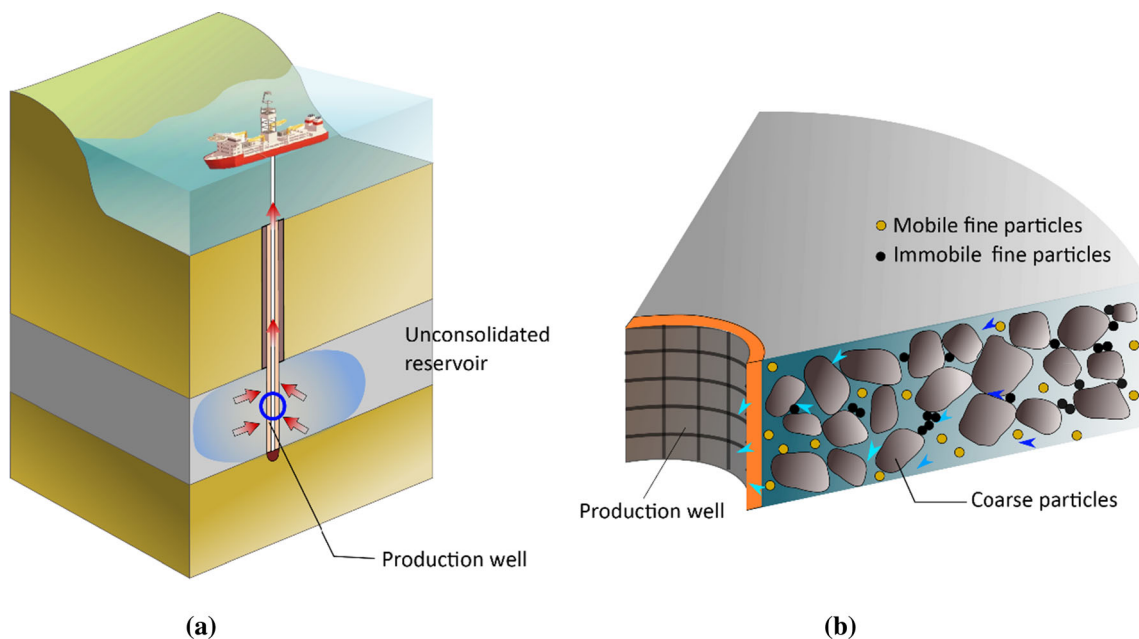


Fig. 2 A schematic illustration of sand production from an unconsolidated reservoir (a). The induced near-wellbore sand production is detailed in (b) (colour figure online)

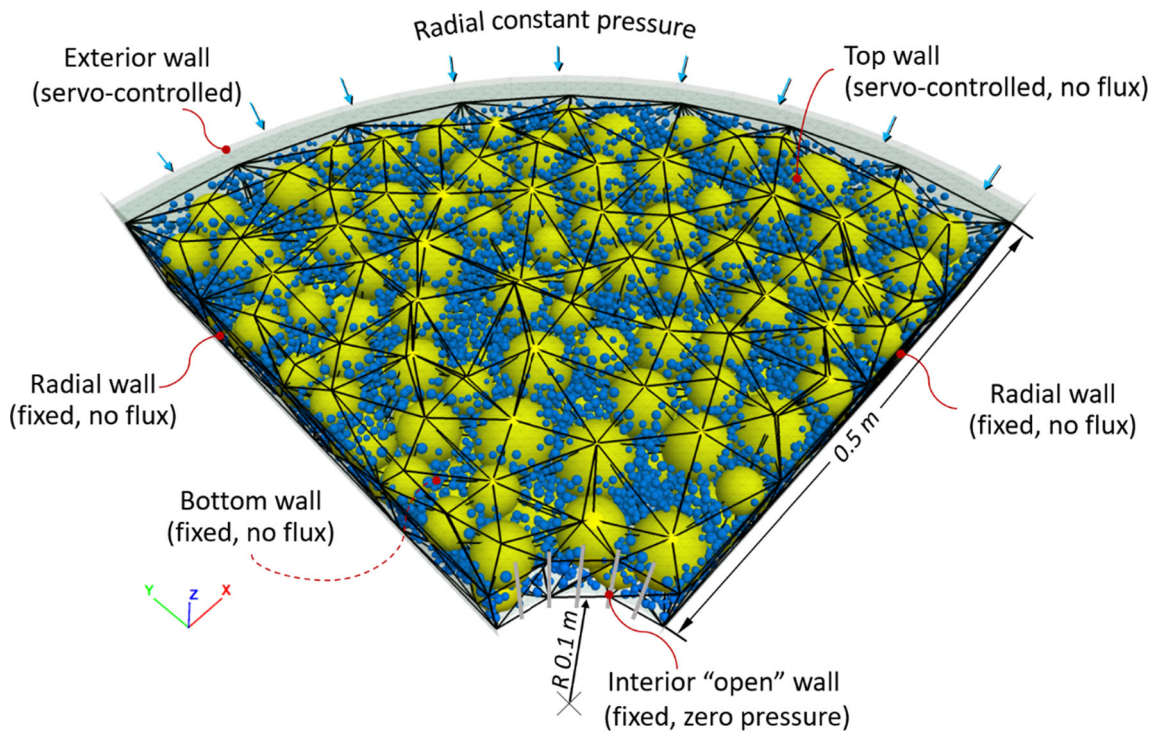


Fig. 3 The sand production model composed of coarse particles (in yellow) and fine particles (in blue), and the boundary conditions set at the walls. The fluid mesh is outlined with black lines. For better visualization, the top wall is made transparent. The bottom wall is covered by the particles and thus unseen. The interior wall is composed of five sub-walls to remain open for fine particles only (colour figure online)

For a fine particle, the drag force exerted by the fluid is computed as:

$$f_d = \frac{4}{3} \pi r^3 \frac{f_b}{(1 - \phi)} \tag{8}$$

where r is the particle radius, and f_b is the drag force per unit volume in the fluid element that the particle occupies:

$$f_b = \beta U, U = \bar{u} - v \tag{9}$$

where β is a coefficient, and U is the average relative velocity between the particles and the fluid, v is the fluid velocity, and \bar{u} is the average velocity of all particles in a given fluid element, defined as:

$$\bar{u} = \frac{1}{N} \sum_j u_j \tag{10}$$

where the sum is over all particles existing in a fluid element, and N is the number of particles.

The coefficient β is calculated in two ways depending on the porosity of the fluid element [38]. According to [38], when the porosity ϕ is less than 0.8, the interaction of particles significantly affects particles' motion and therefore cannot be neglected. Accordingly, β is deduced from well-known Ergun equation [13] for the packed bed:

$$\beta = \frac{(1 - \phi)}{d^2 \phi^2} [150(1 - \phi)\mu + 1.75\rho_f \bar{d}|U|] \quad \phi < 0.8 \tag{11}$$

where ρ_f is the density of the fluid, $|\cdot|$ returns the magnitude of a vector, and \bar{d} is the average diameter of the fine particles staying in the fluid element, defined as:

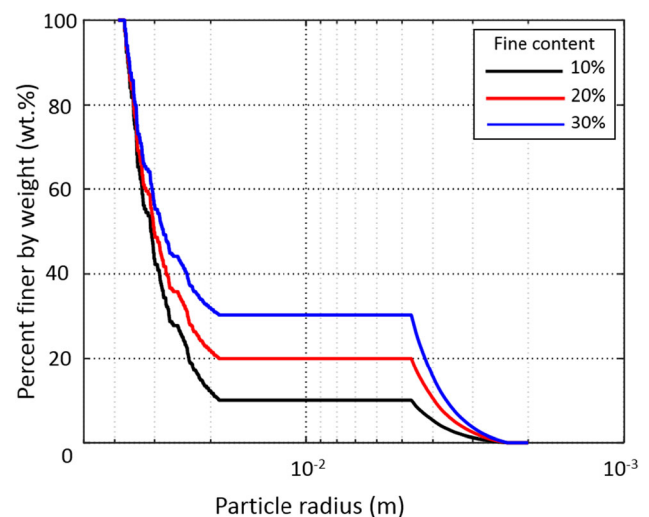


Fig. 4 Particle size distributions of the numerical specimens with different fine contents

Table 1 Model parameters in the numerical model

Parameter	Value
Average radius of coarse particles	28.0 mm
Average radius of fine particles	3.45 mm
Particle density	2650 kg/m ³
Coefficient of inter-particle friction	0.6
Rolling resistance coefficient	0.1
Normal stiffness of coarse particles	5.25 × 10 ⁷ N/m
Normal stiffness of fine particles	7.25 × 10 ⁶ N/m
Normal-to-shear stiffness ratio	2
Normal stiffness of wall	1.0 × 10 ⁸ N/m
Shear stiffness of wall	5.0 × 10 ⁷ N/m
Porosity	0.42 (10% fine content) 0.34 (20% fine content) 0.24 (30% fine content)
Fluid density	1000 kg/m ³
Fluid viscosity	1.0 cp

$$\bar{d} = \frac{1}{N} \sum_j d_j \quad (12)$$

where the sum is over all particles in a given fluid element.

For high porosity ($\phi \geq 0.8$), β is derived from the corrected nonlinear drag force exerted on a spherical particle by a fluid [40]:

$$\beta = \frac{4}{3} C_d \frac{|\mathbf{U}| \rho_f (1 - \phi)}{\bar{d} \phi^{1.7}} \quad \phi \geq 0.8 \quad (13)$$

where C_d is a turbulent drag coefficient defined according to the Reynolds number:

$$C_d = \begin{cases} \frac{24(1 + 0.15R_{ep}^{0.687})}{R_{ep}} & , R_{ep} < 1000 \\ 0.44 & , R_{ep} \geq 1000 \end{cases} \quad (14)$$

where

$$R_{ep} = \frac{|\mathbf{U}| \rho_f \bar{d}}{\mu} \quad (15)$$

3 The numerical model

3.1 Model setup

Figure 2 illustrates a vertical production well in an offshore unconsolidated reservoir consisting of un-cemented and gap-graded sediment. As shown in the close up (Fig. 2b), a radial flow towards the wellbore is driven by pressure

drawdown, and meanwhile, migration of fine particles is mobilized and strengthened near the wellbore because of the enforced hydraulic forces and grain detachment. Fines migration near the wellbore is investigated here through a DEM-DFM coupled model, in which we assume: (1) a single-phase incompressible Newtonian fluid in the laminar flow regime, and (2) isotropic in situ stresses. As shown in Fig. 3, the wellbore with a radius of 0.1 m is drilled through the sediment. We concentrate on the horizontal movement of fine particles towards the well, and thus consider a horizontal ring-shaped slice of the sediment with a thickness of 0.105 m and an exterior radius of 0.6 m to represent the situation at a certain depth. Taking the advantage of the axisymmetric conditions, we simulate one quarter of the entire model for efficiency. The computational regime is enclosed by six walls. The two radial walls and the bottom wall are fixed, and the top wall and the exterior wall are subjected to a servo-controlled mechanism to maintain a constant effective confining pressure (i.e. 5 MPa in the baseline simulation, approximating a well segment at about 500 m below the seafloor). The confining pressure affects the porosity of the matrix and thus the mobility of fine particles in the matrix. Therefore, the effect of the confining pressure is studied and discussed in Sect. 5.4. The interior wall at the wellbore is modelled by five separated and fixed sub-walls to represent an open well segment that allows inflow of fine particles and meanwhile blocks coarse particles. The boundary conditions associated with the flow analysis are configured so as to trigger possible fines migration under a radial flow. The pore pressure is 2 kPa (in the baseline simulation) at the outer circumferential wall, and 0 kPa at the inner circumferential wall. No flux is allowed on the walls except the two circumferential walls and no fine sands across the outer boundary due to the limit of the model size. Given the width of the ring model (i.e. 0.5 m), the near-wellbore hydraulic gradient in the radial direction (defined as the total head drop per unit length) is about 0.4 by ignoring the velocity head. Note that the pressure drawdown during production from a deep well is much higher (e.g. generally between 2 and 5 MPa). Since we use a small near-wellbore model rather than a full-scale reservoir, we can only configure the model according to the near-wellbore gradient that is controlled by the pressure difference between the outer and inner circumferential walls. To avoid segregation and initial heterogeneity of specimens during consolidation, we apply no gravity and buoyancy to the particles, and thus ignore small variation in the stresses along the small thickness of the sediment. The sediment surrounding the wellbore is gap-graded and consists of two groups of particles in order to represent the worst case. The radius ranges from 18.9 to 37.2 mm for the coarse particles, and from 2.33 to 4.62 mm for the fine particles, both following

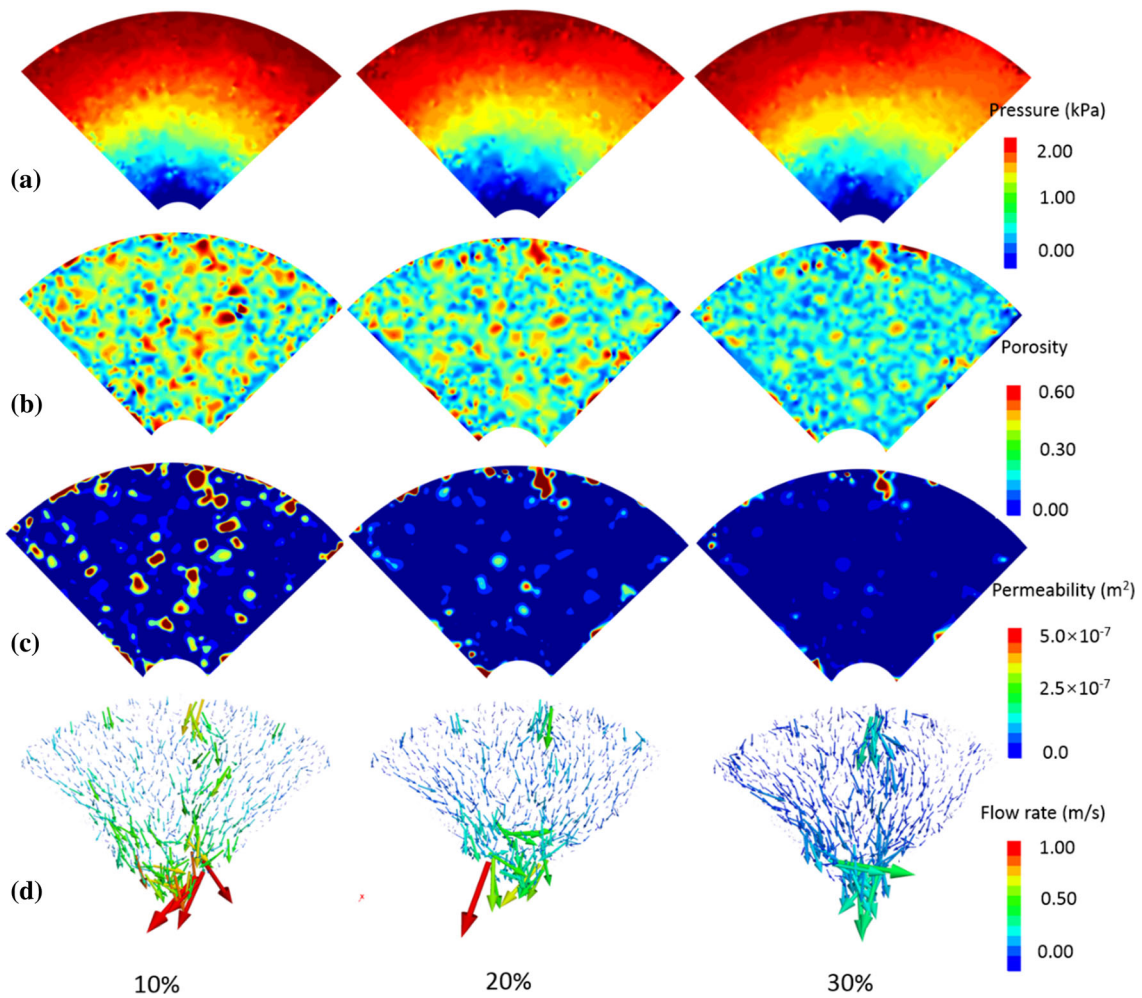


Fig. 5 The effect of the fine content on the initial pressure field (a), the porosity (b), the permeability (c) and the flow rate (d) before fines migration. The velocity vectors are colour coded with different sizes according to the magnitude of the velocities. The fine content is set 10% (the left column), 20% (the middle column) and 30% (the right column)

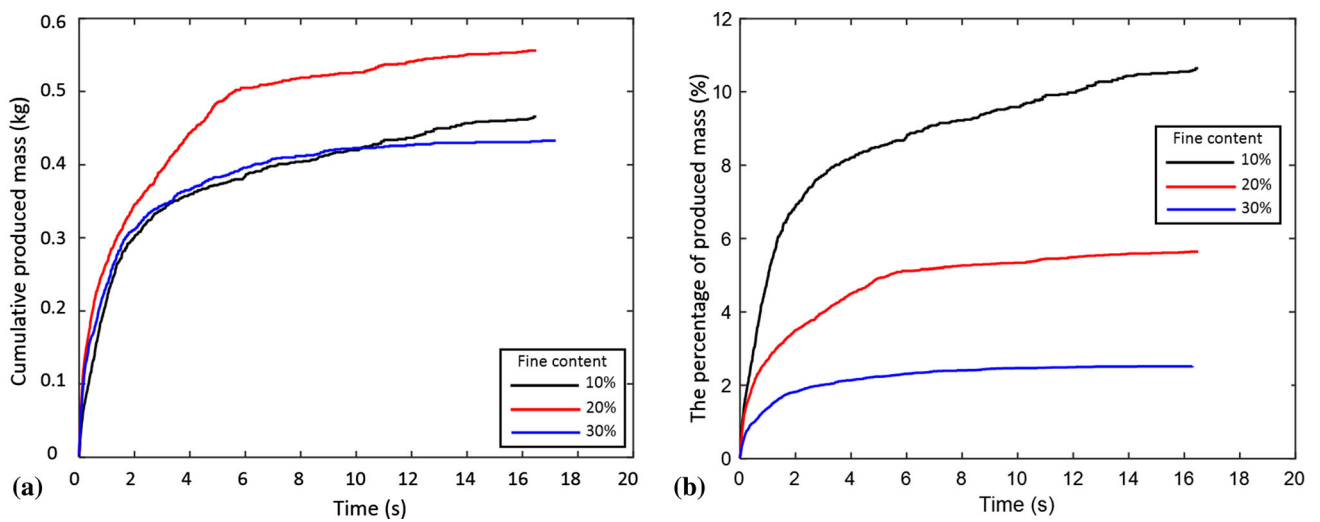


Fig. 6 The produced mass (a), and the percentage of produced mass (b) under different proportions of fine sands

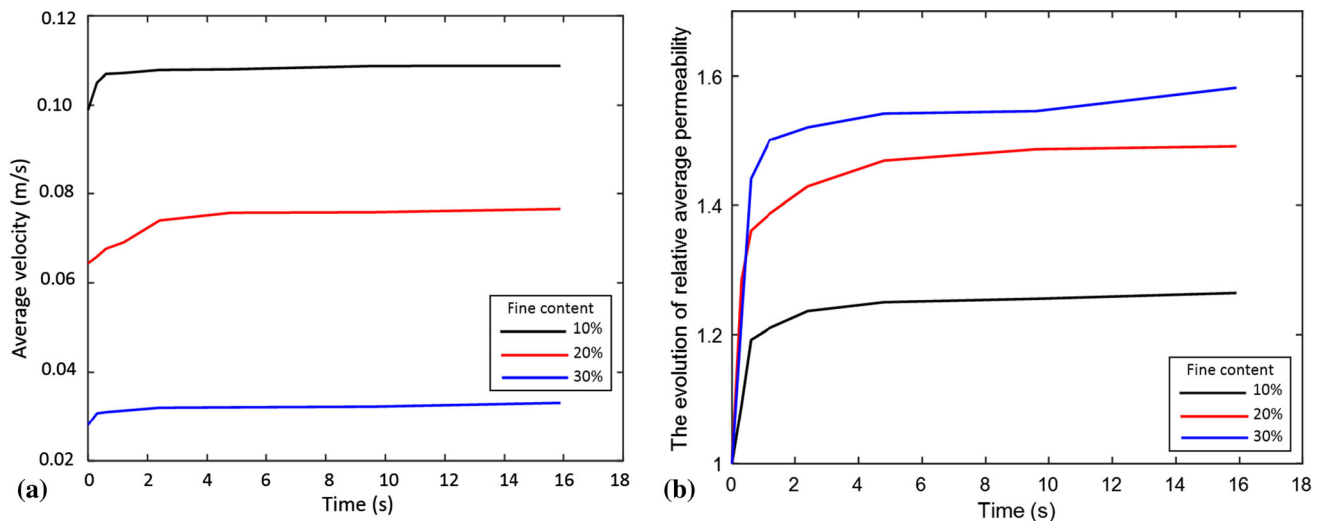


Fig. 7 The variation of the average fluid velocity (a), and the evolution of relative average permeability (b) over time under different fine contents

a linear distribution. The radius of the coarse particles is on average 8 times larger than that of the fine particles so as to enable fines migration process within limited simulation time. This coarse-to-fine size ratio falls into a normal range (i.e. 5 to 10) widely selected in experiments and numerical simulations for feasible studies of fines migration [9, 35, 42]. The fine content (i.e. defined as the percentage in mass of the fine particles) is varied at 10%, 20% and 30% with a fixed number of coarse particles (i.e. 149 in this study), resulting in three specimens with different total numbers of particles, i.e. 8487, 18,967 and 32,698 with the fine content varying from low to high. Figure 4 presents the particle size distributions of three numerical specimens. The rolling resistance linear model is used to account for the effect of irregular shapes of constituent particles on the mechanical behaviour of the sediment [44]. The input parameters of the model are listed in Table 1.

3.2 Simulation procedure

The simulation of fines migration is proceeded in three consecutive steps: specimen generation, specimen consolidation and flow field activation.

In the first step, a granular assembly is generated by using the procedure of particle expanding/shrinking. Initially, a specimen with 32,707 particles and linear radius distribution ranging from 3.3 to 6.7 mm is generated in the space of a quarter of the ring enclosed by six walls. We randomly select 149 particles as coarse particles and gradually enlarge their radius to a range of 18.9 to 37.2 mm in 20 cycles. Meanwhile, we slowly reduce the radius of the remaining particles to a range of 2.33 to 4.62 mm. Subsequently, the model reaches a small average

convergence ratio (0.001) after a number of time steps indicating the completeness of the first step.

In the second step, the interior wall is replaced by five isolated thin cylindrical walls to allow migration of fine particles. We randomly remove some fine particles according to a specified fine content (i.e. 10%, 20%, or 30%). A pre-selected confining pressure (e.g. 5 MPa in the baseline simulation) is applied on the exterior wall and the top wall with all other walls being fixed to consolidate the specimen. Consolidation process terminates after sufficient time steps (i.e. 5000 time steps in our model) required to approximately reach force equilibrium. During consolidation, the skeleton formed by the coarse particles deforms and some of the fine particles could start carrying static forces.

In the last step, a radial inflow through the specimen is activated by imposing a pressure difference between the exterior and interior boundaries, while all other boundaries are set impermeable. Figure 5 presents the initial distributions (at the moment when the radial flow is activated) of the pressure, the porosity and the permeability, and the fluid velocity vectors obtained from the model by varying the fine content from 10 to 30%. As shown in Fig. 5a, a radial pressure drop is evident under all specimens with little effect from the fine content, since the pressure field is primarily controlled by the boundary pressures which are identical in all specimens. As shown in Fig. 5b and c, pore-scale heterogeneity in the porosity and the permeability is well captured by the model particularly in the specimen with low fine contents where local variations are remarkable. In all specimens, the flow velocities of individual fluid cells are neither uniform in the magnitude nor in the direction. The fluid favours some certain paths where the velocity is higher than that of the proximity due to large

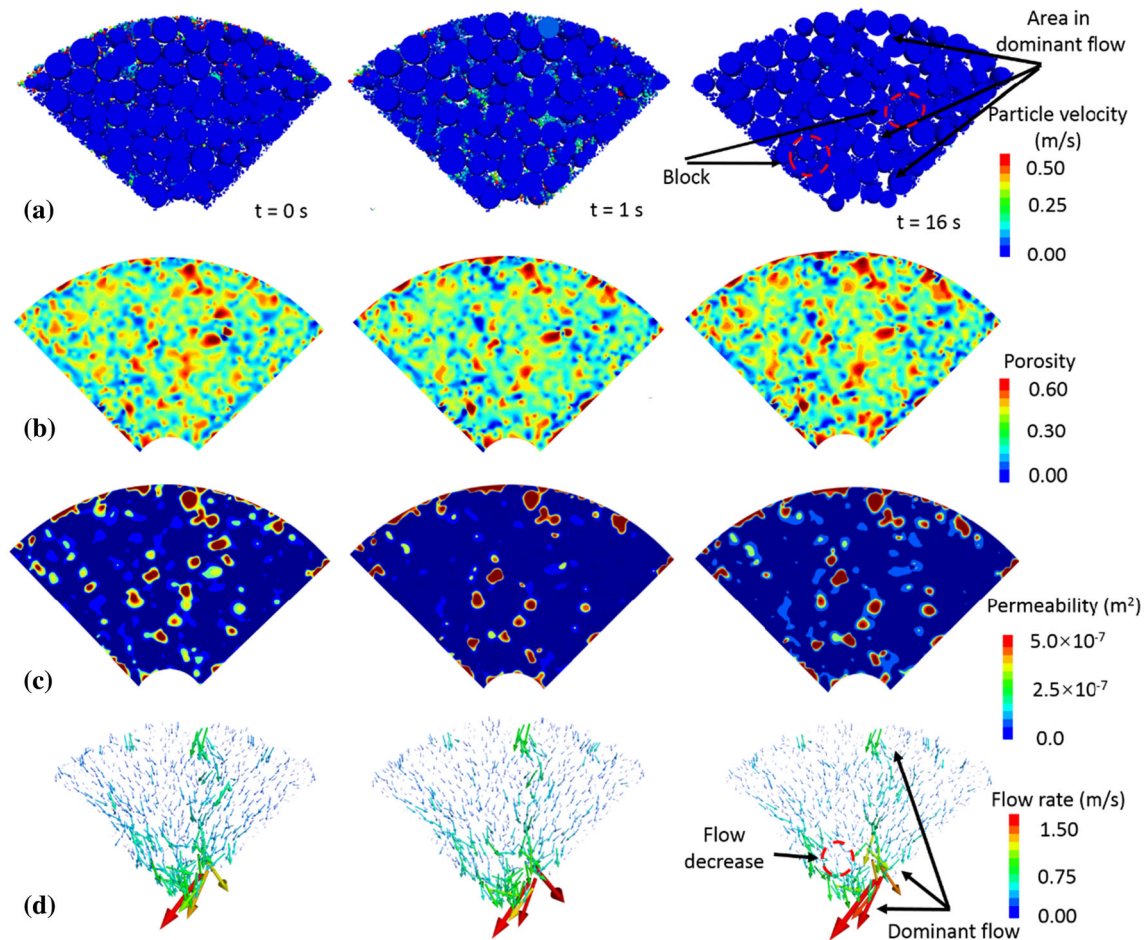


Fig. 8 The particle migration (a), the evolution of porosity (b), the permeability (c) and the flow rate (d) of model with 10% fine content

local pores. However, in general, an overall radial flow is formed with increase in overall velocity towards the wellbore.

4 Simulation results

4.1 Cumulative fines production

Figure 6 presents the cumulative mass of fine particles running out of the model (i.e. the cumulative fines production mass) and the percentage of produced fines (i.e. ratio of mass of produced fines to total mass of fines) under different proportions of the fine particles. In general, the cumulative mass increases rapidly in the first several seconds, then keeps increasing at a declining rate and gradually levels off at the end. Interestingly, the model with 20% fine content produces the maximum volume of fine particles, while the cumulative fines production curves in the cases with 10% and 30% fine contents do not vary significantly. The produced fine particles are 10.87%, 5.64%

and 2.54% in mass of the total fine particles in the case with the fine content of 10%, 20% and 30%, respectively. The critical value of the fine content is further discussed in Sect. 5.

The flow velocity is averaged through all pores, and the resulting average velocity is presented in Fig. 7a. The time history of the average flow velocity resembles the cumulative fines production curve. In the initial stage, the average flow velocity increases rapidly as the fines production mass increases. Subsequently, the increasing rate declines as the fine particles migrate towards the wellbore and partially jam in the pores. The flow velocity decreases with the increase in the fine content because of the reduction in the porosity and the permeability over time due to retention of the fine particles. This implies that the flow velocity is not the only factor of fines migration and production.

The pore-scale permeability computed from Eq. (2) is also averaged through all pores, and the evolution of the average permeability scaled by the initial value is plotted in Fig. 7b. The scaled permeability increases over time under

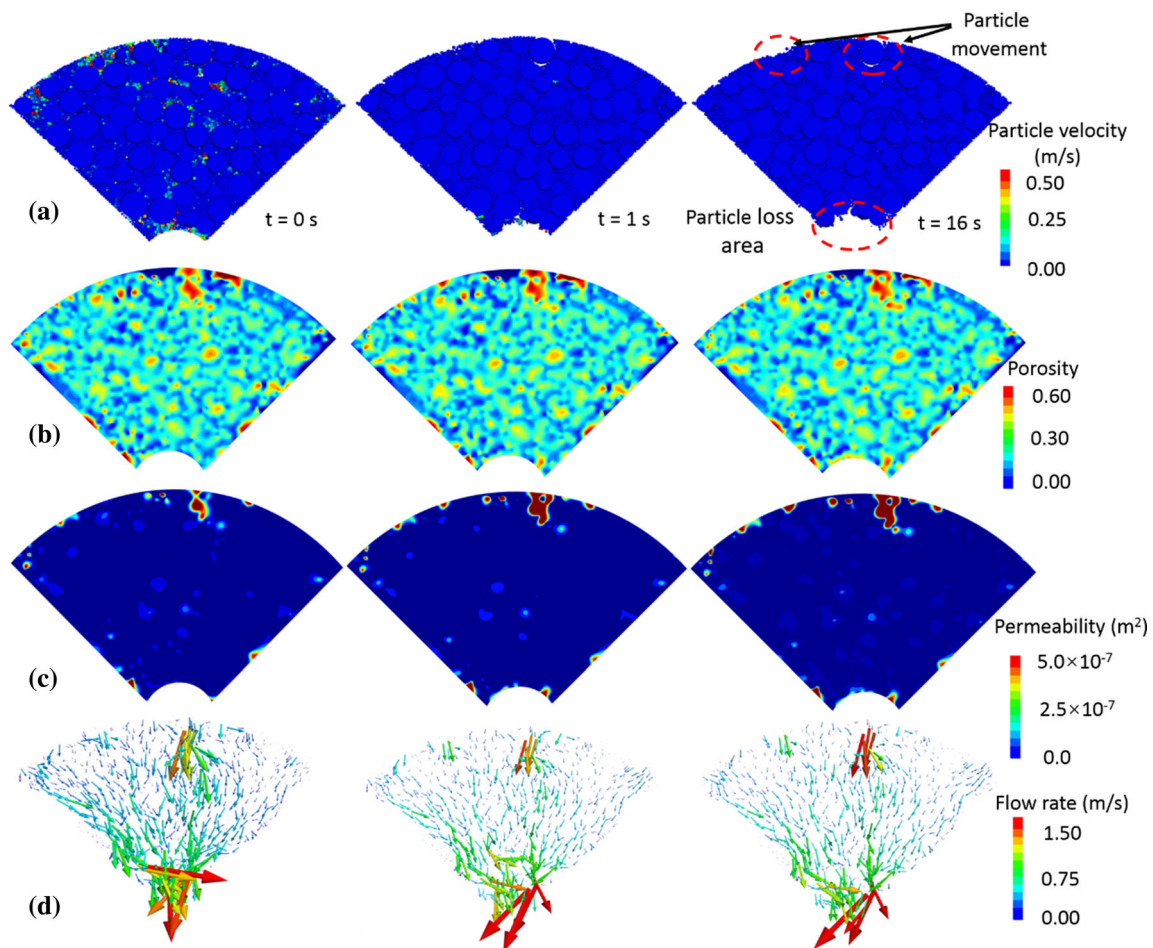


Fig. 9 The particle migration (a), the evolution of porosity (b), the permeability (c) and the flow (d) of model with 30% fine content

any fine content, indicating that the overall porosity of the matrix increases due to fines migration. The rise in the scaled permeability is increasingly remarkable as the fine content increases.

4.2 The role of fine particles

Figure 8 shows the particle movement in the process of fines migration in the case of low fine content (i.e. 10%). Note that the flow pathway does not necessarily correspond to the region of high permeability since the flow rate of fluid is affected by not only the permeability but also the pore connectivity. Initially, fine particles are evenly distributed inside the skeleton formed by coarse particles. Driven by the radial flow, fine particles move towards the wellbore. A large number of fine particles are washed away over time, and the preferred channel is widened due to scouring (Fig. 8). The rate of fines production decreases, because there is no continuous supply of fine particles along the preferred channel, and meanwhile, fine particles elsewhere settle mostly in the pores due to local reduction

of flow velocity. Under field conditions, a continuous fines production is possible in the cases of low fine content as long as adequate and sustaining supply of fines production is ensured.

As the fine content increases up to 30% (see Fig. 9), the majority of pores formed by the coarse particles are densely packed by fine particles. The flow paths of fluid are largely blocked by the increased amount of fine particles. Although the fine particles are adequate for a sustaining fines migration and production process, they are largely immobile in the pores (see Fig. 9a–c) due to the reduced fluid velocity and aggravated jamming of fine particles. Consequently, the loss of fine particles mainly takes place near the wellbore with very limited movement of particles elsewhere.

4.3 Spatial migration pattern of fine particles

As illustrated in Fig. 10, we delineate the model into three zones in the radial direction ($L1$ – $L3$), and compute the variation ratio in mass of fine particles in each zone

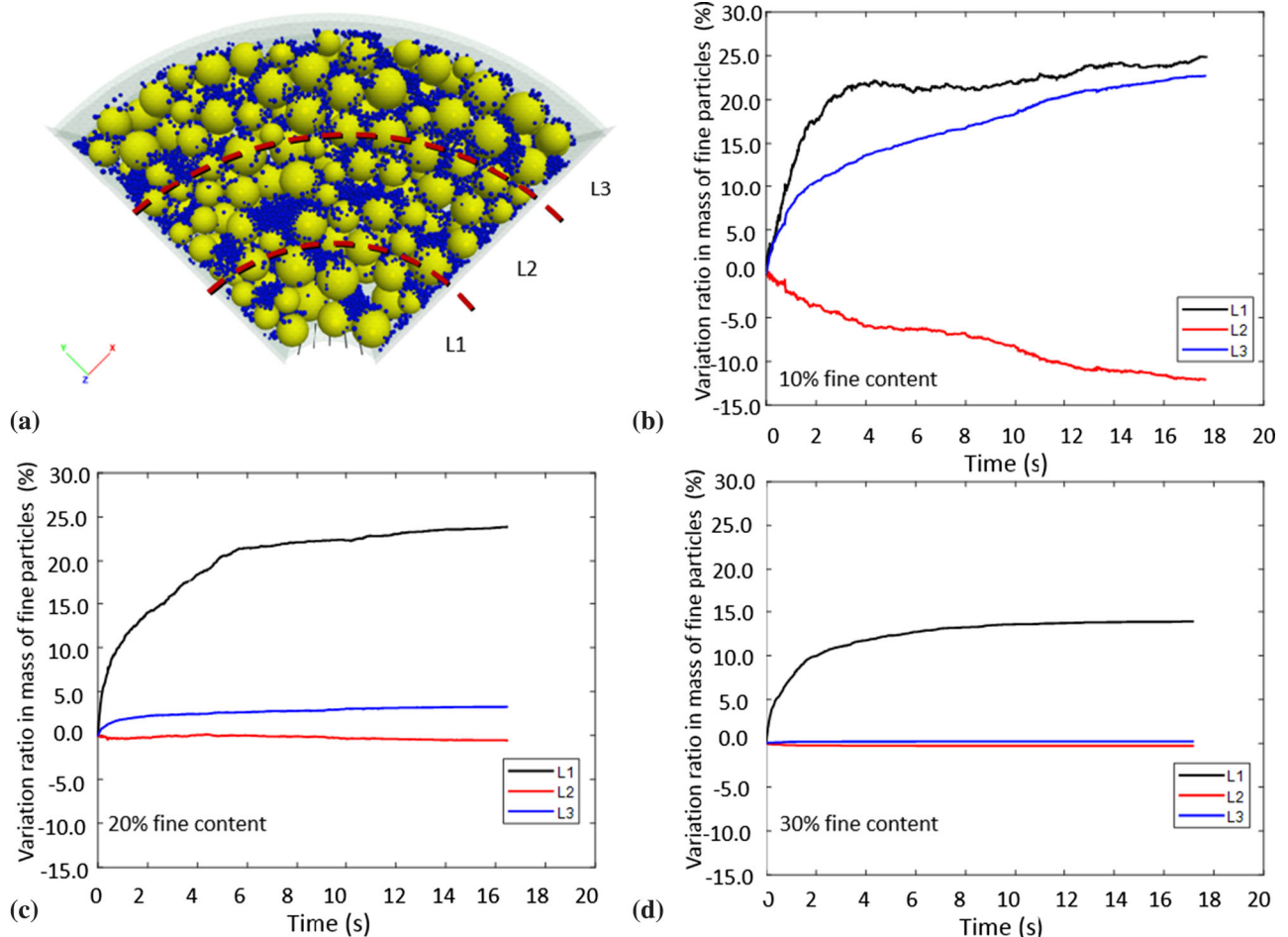


Fig. 10 Fine sand migration in different zones delineated in the model. The division of three zones (a) and the corresponding results (b–d) with low to high fine content

(negative for increase). As shown in Fig. 10b, in the case of low fine contents, the ratio of the fine loss in zone *L1* increases rapidly over time in the early stage and then gradually stabilizes at about 22%. Similarly, fine particles migrate away from zone *L3* due to the radial inflow but at lower rate than that in zone *L1*. Zone *L2* receives more fine particles from *L3* and passes less to zone *L1*; as an overall effect, fine particles are retained and accumulate in zone *L2*, leading to a mass gain in the zone. As the fine content increases up to 20% (see Fig. 10c), the mass loss does not significantly vary in zone *L1* in comparison with the case with 10% fine content, while less fine particles migrate from zone *L3* to *L2* due to decreased porosity and flow velocity so that the variation ratio remains low in zones *L2* and *L3*. As shown in Fig. 10d, in the case of high fine content (i.e. 30%), the migration of fine particles is further restricted by low porosity, which causes descending of the variation ratio in zones *L2* and *L3*. Meanwhile, the mass loss is reduced in zone *L1* as well. Regardless of different initial fine contents, the most loss of fine particles takes

place in the interior zone (*L1*) adjacent to the wellbore, followed by exterior zone distant from the wellbore (*L3*). In the contrast, mass gain is noted in the middle zone (*L2*), which serves like a barrier layer of fines migration. This is consistent with experimental observations [39], and explains the reason of descending production rate of fine particles over time [33]. The influence of the barrier layer is further discussed in Sect. 5.

Figure 11 shows the variation of force chains in the process of fines production. In the case with 10% fine content, fine particles are initially dispersed in pores formed by coarse particles, which have few contacts with other particles. The force chains are rather coarse and mainly contributed by the coarse particles. Driven by the flow, fine particles start moving through the pores. Some of them go through, while the others are retained in pores gaining contacts, indicated by the gradually densified force chains. Different from the case of low fine contents, dense force chains are noted in the case with 30% fine content. This indicates that fine particles are densely packed in

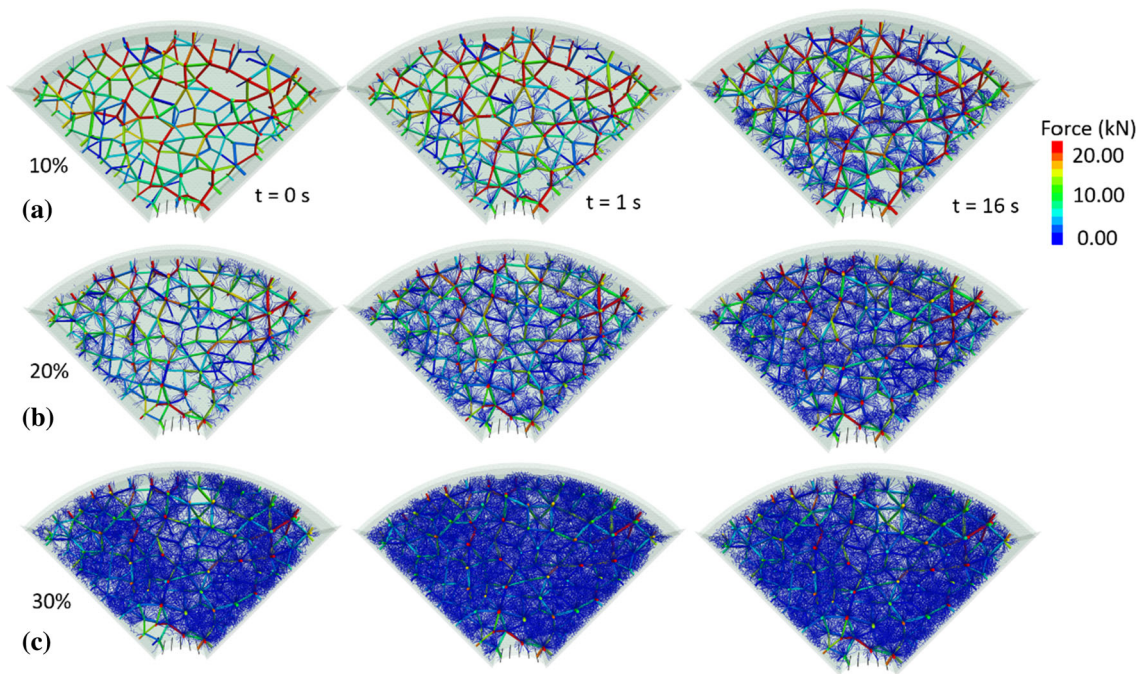


Fig. 11 Different states of contact force chains during sand production in models with different proportions of fine sands. The force chains vary in thickness and colour in proportion to the magnitude of forces

pores and are difficult to move. Similarly, the force chains are densified over time as fine particles migrate through the pores along with the fluid flow and further jam in the throats of pores.

To quantify the variation in the number of fine particles that carry forces, Fig. 12 presents the percentage of fine particles with different coordination numbers at different times. Initially, most of fine particles are floating (identified by coordination numbers smaller than 3) in particular at low fine content, and the floating particles reduce over time as fine particles migrate.

5 Discussion

5.1 The barrier layer

To further reveal the formation mechanism of the barrier layer, we divide the model into five zones evenly from the wellbore to the exterior boundary. The thickness of each zone is 0.1 m. The porosity in every zone before and after fines migration and production is presented in Fig. 13. The overall porosity of the model increases as a result of fines migration and production. However, local reduction in the porosity is noted in the middle zones, and such reduction indicates the approximate position of the barrier layer. In the model with 10% fine content, the barrier layer with reduced porosity is between 0.2 and 0.4 m from the wellbore, while it locates from 0.4 to 0.5 m away from the

wellbores in the models with higher fine contents (i.e. 20% and 30%). This indicates that the barrier layer approaches to the wellbore as the particle mobility is improved with a decreased fine content. Note that the barrier layer affects a long-term production in two different ways. On one hand, it reduces the flow rate and affects the extraction efficiency by decreasing porosity. On the other hand, a stable barrier layer helps to weaken the migration of fine particles and prevent long-term fines production. It should be noted that the location and the size of the barrier layer are affected by the numerical setting. Under field conditions with a continuous supply of fine particles at the outer boundary, we consider that the barrier layer will still form as the fine particles migrate towards the wellbore and the barrier layer will extend farther away from the wellbore as fine particles continuously move in and settle in the pores.

5.2 The critical fine content

The numerical results indicate that the presence of fine particles affects fines migration and production through two competing mechanisms. First, the fine particles provide the source of fines production. Second, they may block the voids, and decrease the porosity of the sediment and in turn the flow rate. The first mechanism causes an increasing fines production with the increase in the fine content, while the second works for the opposite. This indicates a possible existence of a critical fine content, which results in the maximum fines production. Sufficiency

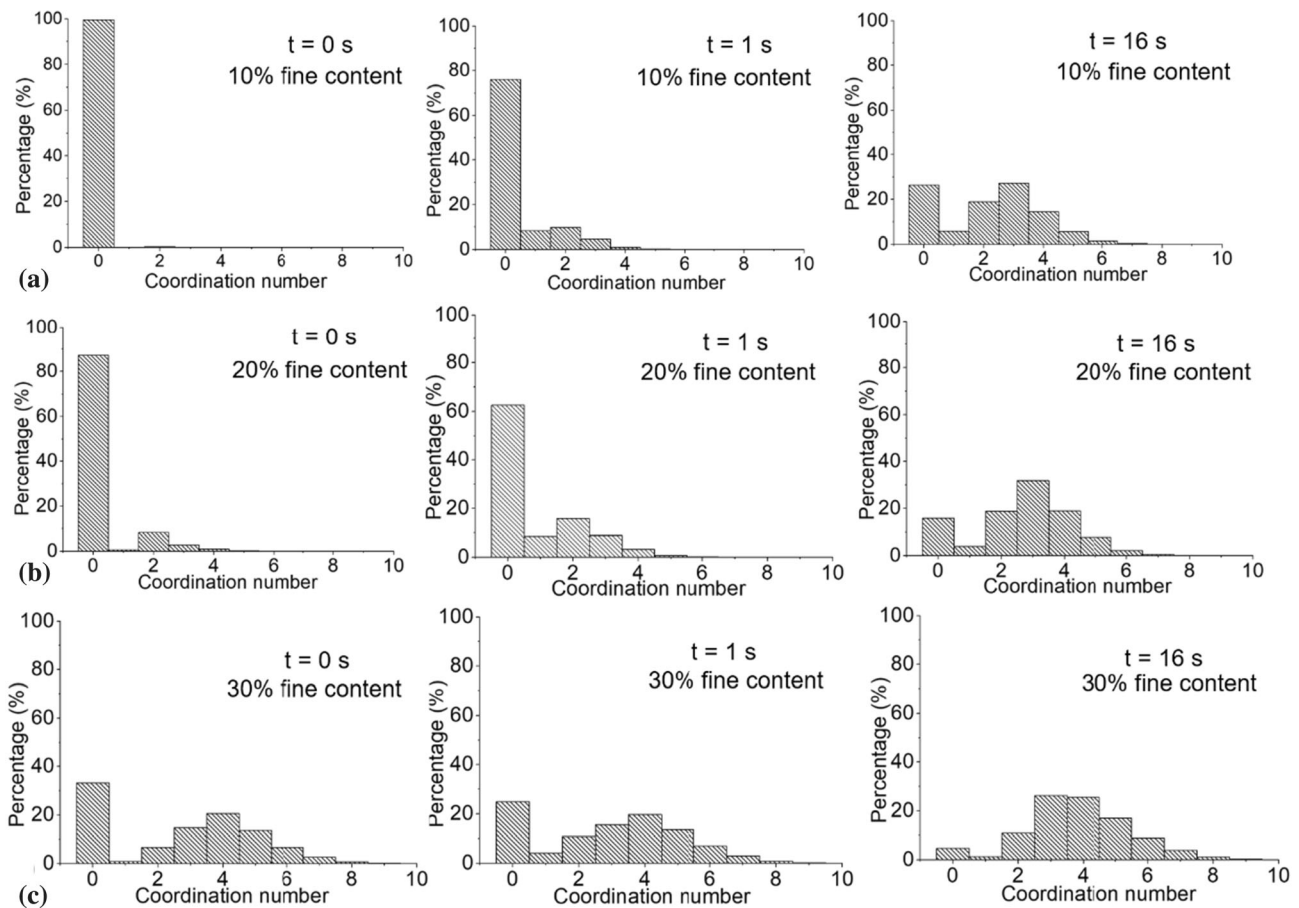


Fig. 12 The percentage variation of coordination number of every model with different fine contents: (a) 10% fine content, (b) 20% fine content and (c) 30% fine content

of fines production source dominates fines migration and production, when the fine content is lower than the critical value; otherwise, the blocking effect of fine particles dominates. This explains the fact that the case with an intermediate fine content produces the most severe fines migration and production than those with lower or higher fine content as shown in Fig. 6. According to our baseline simulation, the critical fine content is around 20%. It should be noted that the critical value is subjected to change under different circumstances. As for the effect of fine content on the properties of a granular sample, Zhang et al. [44] also indicated the existence of a critical fine content at which the sample experiences the transition between the state of “fines in sand” and the state of “sand in fines”. Moreover, this is also consistent with the results of many experiments [8, 25]. The possible value of the critical fine content is likely affected by the fine to coarse particle size ratio. The decrease in such a ratio promotes the loss of fines due to enlarged pore throat size generally [45]. Accordingly, the critical fine content likely increases.

5.3 The effect of the hydraulic gradient

To investigate the effect of the hydraulic gradient, the case with 10% fine content is re-simulated by lowering the pressure on the exterior boundary from 2 (in the baseline simulation) to 1.0 kPa and 0.1 kPa with the other parameters being the same as the baseline simulation. Figure 14 presents fines production curves under different hydraulic gradients. It is evident that the mass of migrated fine particles is positively correlated with the pressure gradient. Some abrupt increases are observed in the fines production curves. According to the study of Zhang et al. [45], jamming (i.e. forming arch structures with particles) is one of the forms of pore blocking. The phenomenon of the abrupt increase in fines production may be caused by a jamming failure due to disturbance. During the process of fines migration in gap-graded sediment, some fine particles form an arch structure with the support of coarse particles, which blocks the pores and prevents the loss of other fine particles. However, this structure is unstable, when the fluid flow changes or particles collide, the arch structure will

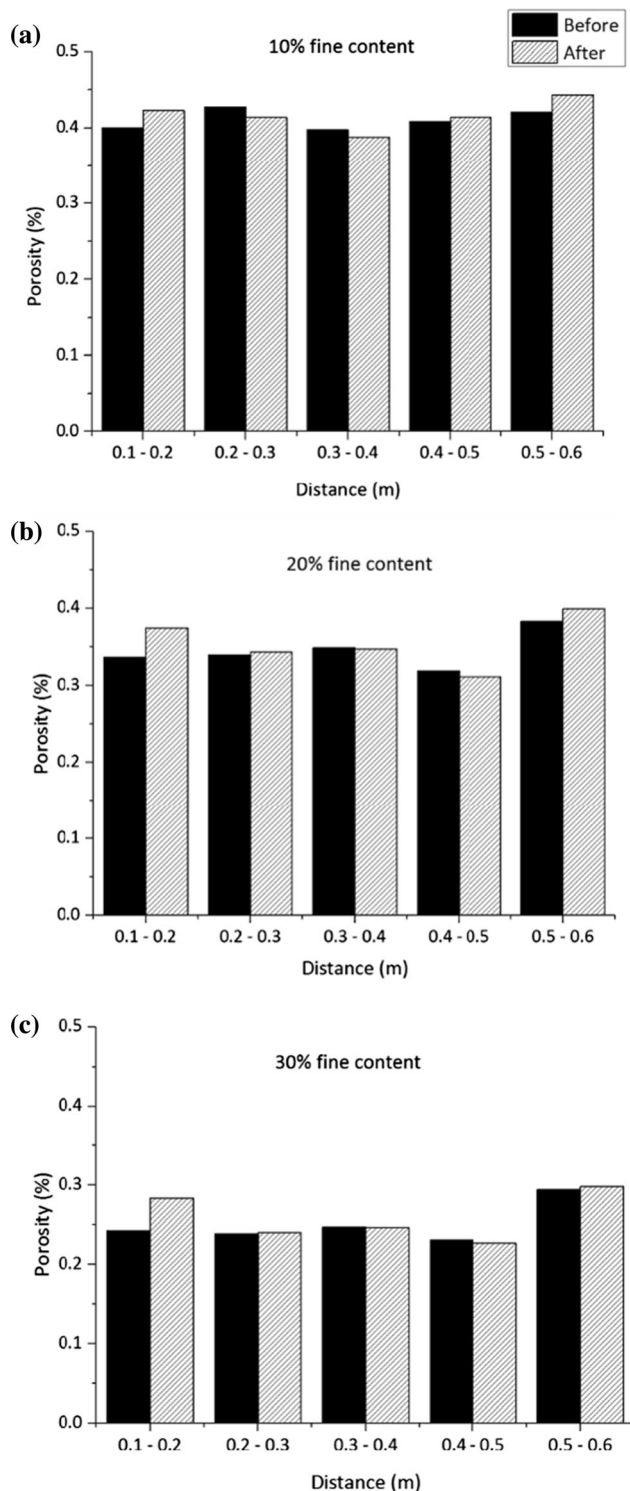


Fig. 13 The porosity variation of every layer in the models with different fine contents: (a) 10% fine content, (b) 20% fine content and (c) 30% fine content

collapse, and the fine particles in the pores will be carried away by flow suddenly.

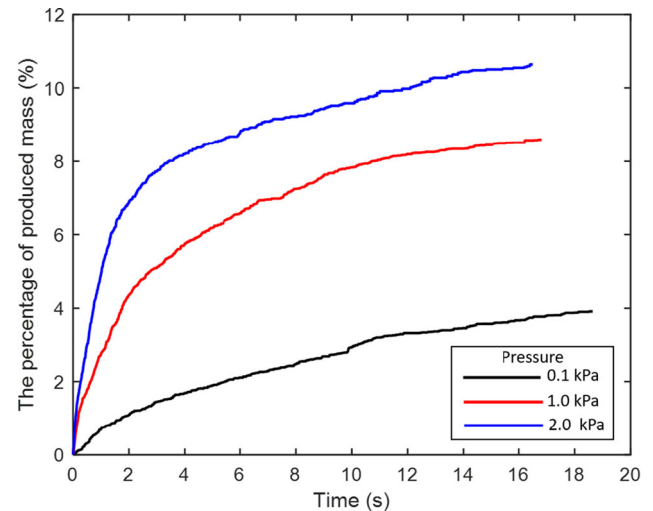


Fig. 14 The percentage of produced mass under different hydraulic pressure on the boundary

5.4 The effect of the confining pressure

Fines migration will be affected by the confining pressure in two aspects. As the confining pressure increases, the porosity of the unconsolidated reservoir reduces, and meanwhile, the fine particles have to overcome higher frictions to move. The simulations are also performed under different confining pressures to mimic fines migration through a wellbore at different depths, while other parameters are the same as baseline model. As shown in Fig. 15, the fines production rate does not vary significantly in the early stage as the confining pressure changes, because an incremental confining pressure does not significantly alter the initial pore structure of a sediment already consolidated under a rather high confining pressure. However, the pressure effect becomes prominent as fines migrate, and the ultimate mass of the produced fine particles decreases as the confining pressure increases. This is due to the fact that the increase in the confining pressure increases the friction between particles, and then reduces the collapse of arches formed as a result of fines migration and clog. In comparison with the case of high fine contents, the case of low fine contents is more sensible to the variation in the confining pressure due to a more porous structure. However, from the point of the loss mass of fines, regardless of different confining pressures, the case with the intermediate fine content (20%) always generates the maximum loss of fine particles.

5.5 The effect of the fluid viscosity

To study the effect of the fluid viscosity, two additional simulations with the fluid viscosity equal to 5 cp and 20 cp were carried out. All other conditions are the same as the

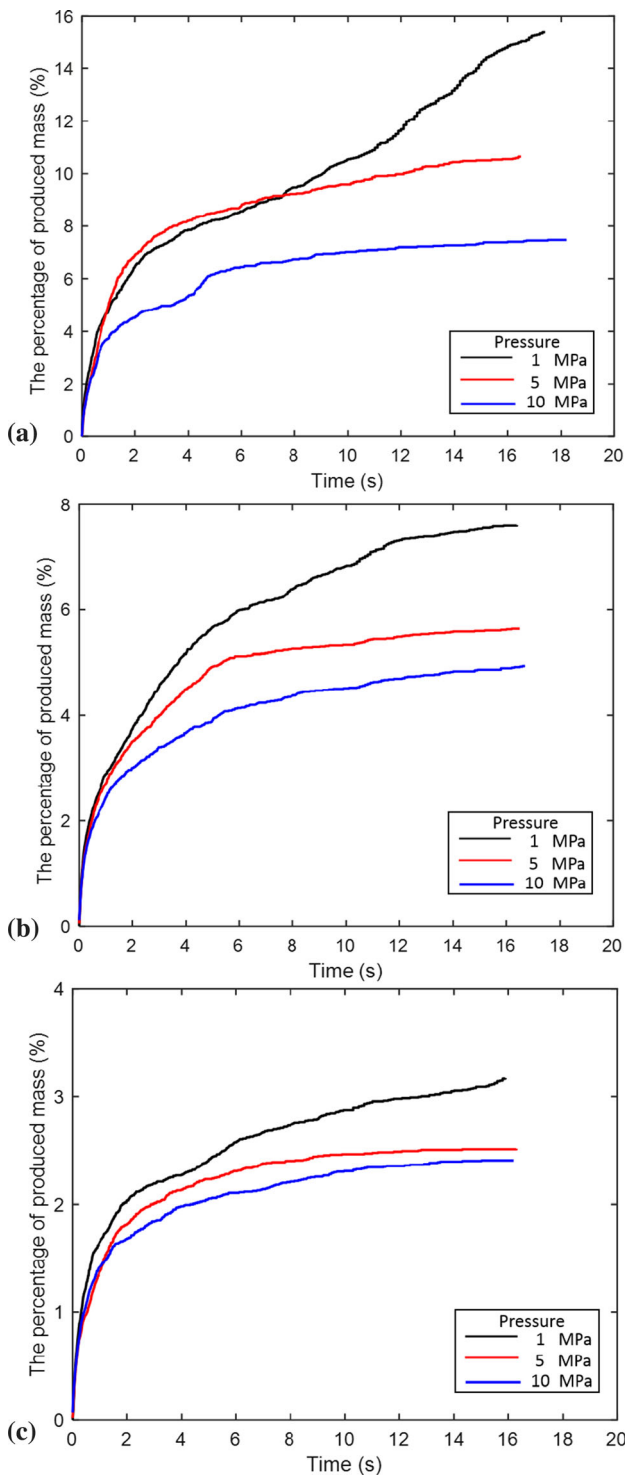


Fig. 15 Relation between the cumulative produced particle mass and time under different confining pressures: (a) 10% fine content, (b) 20% fine content and (c) 30% fine content

baseline case with 10% fine content. The fines production curves are plotted in Fig. 16. The results indicate a negative correlation between fines production and the fluid viscosity. The variation of the fluid viscosity affects the

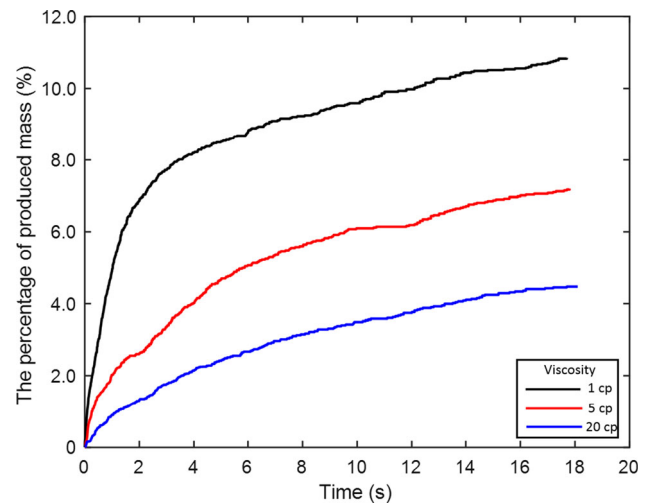


Fig. 16 Relation between the percentage of produced mass and time under different fluid viscosities: (a) 1 cp fluid viscosity, (b) 5 cp fluid viscosity and (c) 20 cp fluid viscosity

results in two ways. On one hand, the increase in the fluid viscosity leads to a decrease in the fluid velocity (Eq. 3) and in turn the drag force (Eq. 9), and therefore slow down the movement of fine particles. On the other hand, the drag force coefficient (β) is positively correlated with the fluid viscosity (Eq. 11). In our model, the first effect dominates. Thus, the drag force decreases as the fluid viscosity increases. This results in an overall decrease in the migration capacity of the fine particles and reduces fines migration and production, as the fluid viscosity increases.

6 Conclusions

This paper investigates production-induced fines migration near a wellbore drilled in an unconsolidated and gap-graded sediment by using a recently developed DEM-DFM coupled scheme. This scheme has capability to naturally capture pore-scale movements of fine particles, and spatiotemporal variations of the porosity and the permeability in the sediment. The influential factors are analysed through parametric studies with emphasis on the role of the fine particles.

Two mechanisms compete as the fine content varies in the sediment. Under a low fine content, fines mainly serve as the fines production source, and therefore, fines production is enhanced as the fine content increases up to the critical value, beyond which fines production is weakened since the blocking effect starts to dominate. The critical fine content is approximately 20% in our baseline simulation, and this value will be affected by a number of parameters, such as the porosity of the skeleton formed by

coarse particles, the confining pressure and the hydraulic gradient .

A barrier layer is likely formed during fines migration due to settling and jamming of fines at the throats of pores, as the fines migrate with the radial flow towards the wellbore. The location of this layer is affected by the fine content. The barrier layer is helpful to slow down or prevent long-term fines production, and however, it could also impede normal production due to reduced permeability in the affected reservoir .

It should be noted that the assumption of incompressible flow in this model becomes less qualified if the gas content in the fluid increases and the fluid bulk modulus deteriorates. Nevertheless, this work provides an efficient numerical tool for coupled fluid–particle interaction and has broad implications to the mechanism of fines migration in unconsolidated reservoirs.

Acknowledgements This work is partially supported by the key innovation team program of innovation talents promotion plan by MOST of China (with grant No. 2016RA4059), the National Natural Science Foundation of China (with grant No. 41772286 and 41877241) and the Fundamental Research Funds for the Central Universities (with grant No. 22120200081).

References

- Al-Shaabi SK, Al-Ajmi AM, Al-Wahaibi Y (2013) Three dimensional modeling for predicting sand production. *J Pet Sci Eng* 109:348–363. <https://doi.org/10.1016/j.petrol.2013.04.015>
- Bear J (1972) Dynamics of fluids in porous media. American Elsevier Pub. Co., New York
- Blanco SF (2015) Learning SciPy for numerical and scientific computing. Packt Publishing, Birmingham
- Boutt DF, Cook BK, Williams JR (2010) A coupled fluid–solid model for problems in geomechanics: application to sand production D. *Int J Numer Anal Methods Geomech* 35:998–1018. <https://doi.org/10.1002/nag>
- Brumby PE, Sato T, Nagao J et al (2015) Coupled LBM–DEM micro-scale simulations of cohesive particle erosion due to shear flows. *Transp Porous Media* 109:43–60. <https://doi.org/10.1007/s11242-015-0500-2>
- Cao SC, Jang J, Jung J et al (2019) 2D micromodel study of clogging behavior of fine-grained particles associated with gas hydrate production in NGHP-02 gas hydrate reservoir sediments. *Mar Pet Geol* 108:714–730. <https://doi.org/10.1016/j.marpetgeo.2018.09.010>
- Chang DS, Zhang LM (2012) Critical hydraulic gradients of internal erosion under complex stress states. *J Geotech Geoenviron Eng* 139:1454–1467. [https://doi.org/10.1061/\(asce\)gt.1943-5606.0000871](https://doi.org/10.1061/(asce)gt.1943-5606.0000871)
- Chang DS, Zhang LM (2013) Extended internal stability criteria for soils under seepage. *Soils Found* 53:569–583. <https://doi.org/10.1016/j.sandf.2013.06.008>
- Chang DS, Zhang LM, Cheuk J (2014) Mechanical consequences of internal soil erosion. *HKIE Trans Hong Kong Inst Eng* 21:198–208. <https://doi.org/10.1080/1023697X.2014.970746>
- Climent N, Arroyo M, Sullivan CO (2014) Sand production simulation coupling DEM with CFD. *Eur J Environ Civil Eng.* <https://doi.org/10.1080/19648189.2014.920280>
- Dallimore SR, Wright JF, Nixon FM (2008) Geologic and porous media factors affecting the 2007 production response characteristics of the JOGMEC/NRCAN/ AURORA Mallik gas hydrate production research well. In: the 6th International Conference on Gas Hydrates. Vancouver, British Columbia, Canada
- Dersoir B, Schofield AB, Tabuteau H (2017) Clogging transition induced by self filtration in a slit pore. *Soft Matter* 13:2054–2066. <https://doi.org/10.1039/c6sm02605b>
- Ergun S (1952) Fluid flow through packed columns. *Chem Eng Prog* 48:89–94
- Fan M, McClure J, Han Y et al (2018) Interaction between proppant compaction and single-/multiphase flows in a hydraulic fracture. *SPE J* 23:1290–1303. <https://doi.org/10.2118/189985-PA>
- Feng AG, Feng BG (2014) Sand production in oil wells prediction method based on data mining technology. In: 2014 Asia-Pacific computer science and application conference. Shanghai, China, pp 97–102
- Ghassemi A, Pak A (2015) Numerical simulation of sand production experiment using a coupled Lattice Boltzmann–Discrete Element Method. *J Pet Sci Eng* 135:218–231. <https://doi.org/10.1016/j.petrol.2015.09.019>
- Gholami R, Aadnoy B, Rasouli V, Fakhari N (2016) An analytical model to predict the volume of sand during drilling and production. *J Rock Mech Geotech Eng* 8:521–532. <https://doi.org/10.1016/j.jrmge.2016.01.002>
- Grof Z, Cook J, Lawrence CJ, Štěpánek F (2009) The interaction between small clusters of cohesive particles and laminar flow: coupled DEM/CFD approach. *J Pet Sci Eng* 66:24–32. <https://doi.org/10.1016/j.petrol.2009.01.002>
- Han Y, Cundall PA (2012) LBM–DEM modeling of fluid–solid interaction in porous media. *Int J Numer Anal Methods Geomech.* <https://doi.org/10.1002/nag>
- Han G, Kwon TH, Lee JY, Kneafsey TJ (2018) Depressurization-induced fines migration in sediments containing methane hydrate: X-ray computed tomography imaging experiments. *J Geophys Res Solid Earth* 123:2539–2558. <https://doi.org/10.1002/2017JB014988>
- Hoek Van Den PJ, Kooijman AP, De Bree P et al (2000) Horizontal-wellbore stability and sand production in weakly consolidated sandstones. *SPE Drill Complet* 15:274–283. <https://doi.org/10.2118/65755-PA>
- Itasca Consulting Group Inc. (2015) PFC3D (Particle flow code in 3 dimensions), Version 5.0, Documentation set of version 6.00.55. Minneapolis, Itasca
- Jang J, Cao SC, Stern LA et al (2020) Potential freshening impacts on fines migration and pore-throat clogging during gas hydrate production: 2-D micromodel study with Diatomaceous UBGH2 sediments. *Mar Pet Geol* 116:104244. <https://doi.org/10.1016/j.marpetgeo.2020.104244>
- JOGMEC (2017) The second MH tests. In: http://www.jogmec.go.jp/news/release/news_10_000243.html,
- Ke L, Takahashi A (2014) Experimental investigations on suffusion characteristics and its mechanical consequences on saturated cohesionless soil. *Soils Found* 54:713–730. <https://doi.org/10.1016/j.sandf.2014.06.024>
- Kenney TC, Lau D (1985) Internal stability of granular filters. *Can Geotech J* 22:215–225. <https://doi.org/10.1139/t86-068>
- Li L, Papamichos E, Cerasi P (2006) A study of mechanisms of sand production using DEM with fluid flow. In: Van Cotthem A, Charlier R, Thimus JF (eds) Multiphysics coupling and long term behaviour in rock mechanics. Eurock06, Liege, Belgium, pp 241–247
- Liu Q, Zhao B, Santamarina JC (2019) Particle migration and clogging in porous media: a convergent flow microfluidics study.

- J Geophys Res Solid Earth 124:9495–9504. <https://doi.org/10.1029/2019JB017813>
29. Muecke TW (1979) Formation fines and factors controlling their movement in porous media. *JPT, J Pet Technol* 31:144–150. <https://doi.org/10.2118/7007-PA>
 30. Papamichos E, Vardoulakis I, Tronvoll J, Skjirstein A (2001) Volumetric sand production model and experiment. *Int J Numer Anal Methods Geomech* 25:789–808. <https://doi.org/10.1002/nag.154>
 31. Rahmati H, Jafarpour M, Azadbakht S et al (2013) Review of sand production prediction models. *J Pet Eng* 2013:1–16. <https://doi.org/10.1155/2013/864981>
 32. Ranjith PG, Perera MSA, Perera WKG et al (2013) Effective parameters for sand production in unconsolidated formations: an experimental study. *J Pet Sci Eng* 105:34–42. <https://doi.org/10.1016/j.petrol.2013.03.023>
 33. Schoderbek D, Farrell H, Hester K et al (2013) “ConocoPhillips gas hydrate production test” Final Technical Report
 34. Shaffee SNA, Luckham PF, Matar OK et al (2019) Numerical investigation of sand-screen performance in the presence of adhesive effects for enhanced sand control. *SPE J* 24:2195–2208. <https://doi.org/10.2118/195686-PA>
 35. Shire T, O’Sullivan C, Hanley KJ, Fannin RJ (2014) Fabric and effective stress distribution in internally unstable soils. *J Geotech Geoenvironmental Eng* 140:04014072. [https://doi.org/10.1061/\(ASCE\)GT.1943-5606.0001184](https://doi.org/10.1061/(ASCE)GT.1943-5606.0001184)
 36. Silpa-Anan C, Hartley R (2008) Optimised KD-trees for fast image descriptor matching. In: *IEEE conference on computer vision & pattern recognition*. IEEE, Anchorage, Alaska, USA
 37. Tang Y, Yao X, Chen Y et al (2020) Experiment research on physical clogging mechanism in the porous media and its impact on permeability. *Granul Matter*. <https://doi.org/10.1007/s10035-020-1001-8>
 38. Tsuji Y, Kawaguchi T, Tanaka T (1993) Discrete particle simulation of two-dimensional fluidized bed. *Powder Technol* 77:79–87. [https://doi.org/10.1016/0032-5910\(93\)85010-7](https://doi.org/10.1016/0032-5910(93)85010-7)
 39. Valdes JR, Santamarina JC (2006) Particle clogging in radial flow: Microscale mechanisms. *SPE J* 11:193–198. <https://doi.org/10.2118/88819-PA>
 40. Wen CY, Yu YH (1966) Mechanics of fluidization. *Chem Eng Prog Symp Ser* 62:100–111
 41. Yan C, Li Y, Cheng Y et al (2018) Sand production evaluation during gas production from natural gas hydrates. *J Nat Gas Sci Eng* 57:77–88. <https://doi.org/10.1016/j.jngse.2018.07.006>
 42. Zhang LM, Chen Q (2011) Seepage failure mechanism of the Gouhou rockfill dam during reservoir water infiltration. *Soils Found* 46:557–568
 43. Zhang D, Gao C, Yin Z (2019) CFD-DEM modeling of seepage erosion around shield tunnels. *Tunn Undergr Sp Technol* 83:60–72. <https://doi.org/10.1016/j.tust.2018.09.017>
 44. Zhang F, Li M, Peng M et al (2019) Three-dimensional DEM modeling of the stress–strain behavior for the gap-graded soils subjected to internal erosion. *Acta Geotech* 14:487–503. <https://doi.org/10.1007/s11440-018-0655-4>
 45. Zhang F, Wang T, Liu F et al (2020) Modeling of fluid-particle interaction by coupling the discrete element method with a dynamic fluid mesh: implications to suffusion in gap-graded soils. *Comput Geotech* 124:1–13. <https://doi.org/10.1016/j.compgeo.2020.103617>
 46. Zhao T (2014) Investigation of landslide-induced debris flows by the DEM and CFD. Ph.D. thesis, St Cross College, University of Oxford, UK
 47. Zhou S, Sun F (2016) Sand production management for unconsolidated sandstone reservoirs. Wiley, Singapore

Publisher’s Note Springer Nature remains neutral with regard to jurisdictional claims in published maps and institutional affiliations.